Influence of Fluorocarbon Chains on the Crystallization Behaviors of Aliphatic Polyurethanes

Kuo-Yu Chen,[1] Jen-Feng Kuo[2]

[1]*Institute of Biomedical Engineering and Material Science, Central Taiwan University of Science and Technology, Taichung, Taiwan*
[2]*Department of Chemical Engineering, National Cheng Kung University, Tainan, Taiwan*

Received 26 January 2008; accepted 21 July 2008
DOI 10.1002/app.29049
Published online 3 October 2008 in Wiley InterScience (www.interscience.wiley.com).

ABSTRACT: The aliphatic polyurethanes were synthesized from either hexamethylene diisocyanate (HDI) and 2,2,3,3-tetrafluoror-1,4-butanediol or HDI and 1,4-butandiol. The crystallization behaviors of the aliphatic polyurethanes were characterized using differential scanning calorimetry, wide-angle X-ray diffraction, and polarized optical microscopy. The effects of fluorocarbon chains on the solubility behavior, microstructure, thermal transition property, crystal morphology, and crystallization behaviors were investigated. The fluorinated polyurethane exhibited a lower viscosity, higher solubility in organic solvents, smaller fraction of ordered hydrogen-bonded carbonyls, and lower transition temperatures than the corresponding fluorine-free polyurethane. The wide-angle X-ray diffraction measurements reflected change of crystal structure with the $(CF_2)_2$ moieties in place of $(CH_2)_2$ moieties. Polarized optical microscopy also revealed that the polyurethanes exhibited a variety of spherulitic texture. The isothermal crystallization process of the polyurethanes was described by the Avrami analysis. The result showed that the Avrami exponent (n) was around 2.5, which suggested the growth of crystal might be spherulite growth corresponding to homogeneous (thermal) nucleation and diffusion control. The crystallization activation energy was estimated to be −130.9 kJ/mol for the fluorinated polyurethane and −276.9 kJ/mol for the fluorine-free polyurethane from Arrhenius form.
© 2008 Wiley Periodicals, Inc. J Appl Polym Sci 111: 371–379, 2009

Key words: polyurethanes; crystallization behavior; fluorocarbon; morphology

INTRODUCTION

Fluorinated polymers have exhibited many interesting properties due to the unique characteristics of the fluorocarbon chains, including high oxygen permeability,[1] good hydrolytic stability,[2] excellent thermal stability and chemical resistance,[2,3] low dielectric constant, low interfacial free energy, and good water and oil repellent.

Some researchers introduced fluorocarbon chains into polyurethanes via fluoro-containing diisocyanate, chain extender, or soft segment to obtain novel functions. For instance, Ho et al.[4,5] synthesized a series of fluorinated polyurethanes by using various fluorinated diols to obtain polyurethanes with surfaces with minimum adhesion. Kashiwagi et al.[6] synthesized polyurethanes containing fluoroalkyl groups in the side chains of hard segments and showed that the *in vitro* thrombus formation was reduced as fluoroalkyl content increased. Tonelli et al.[7,8] utilized a perfluoropolyether as a soft segment to synthesize fluorinated polyurethanes, which exhibits a low coefficient of friction, low-temperature elastomeric behavior, thermal stability, and superior chemical resistance. Santerre et al.[9–11] mixed fluorine-containing polyurethanes with base polyurethanes to improve the biostability and blood compatibility of the base polyurethanes. Hsieh et al.[12] showed that the fluorodiol-containing polyurethanes have a low surface energy and good blood compatibility. Wang and Wei[13,14] studied the effects of soft segment length on the degree of phase separation, thermal behaviors, surface composition, and platelet adhesion properties of fluorinated polyurethanes. In our previous studies,[15] a series of aliphatic fluorinated polyurethanes were synthesized with different fluorinated chain extender. The addition of fluorocarbon chains into aliphatic polyurethanes leads to a reduction in platelet adhesion and activation. Moreover, the more the fluorine is on the surface, the more thromboresistant the material is.

A number of studies have been carried out on the structure, morphology, and properties of polyurethanes. Nevertheless, only a few studies have been published on the crystallization kinetics of polyurethanes. Schacht and coworkers[16] prepared

Correspondence to: K.-Y. Chen (kychen@ctust.edu.tw).

© 2008 Wiley Periodicals, Inc.

poly(ester-urethanes) based on polycaprolactone as a soft segment and studied the isothermal crystallization kinetics of the soft segment continuous phase in the poly(ester-urethanes). Hu and coworkers[17,18] studied the effects of different ionic group contents and counterions on the crystallization behavior of polycaprolactone-based polyurethane ionomers by isothermal crystallization kinetics. MacKnight and coworkers[19] investigated the crystallization kinetics of the polyurethane containing mesogenic units.

In our previous studies,[15] the fluorocarbon chains and the average length of hard segments were found to influence significantly the microstructure, thermal transition property, and surface property of polyurethanes. It is expected that the crystallization behaviors of polymers will have significant influence on their physical properties. However, the effect of fluorine substituents on the crystallization behaviors of polyurethane has not been extensively studied. Moreover, no work has been published on the crystallization kinetics of fluorinated polyurethanes. Thereby, it would appear that the study of the crystallization behaviors of fluorinated polyurethanes might lead to a better understanding of the effect of fluorocarbon chains on the properties of fluorinated polyurethanes.

There is a higher content of fluorine present on the surface and in the matrix of polyurethanes using fluoro-containing soft segment. However, most researchers introduce fluorocarbon chains into polyurethanes via fluorinated chain extender due to the poor availability of fluoro-containing diisocyanate and soft segment. The aim of this investigation was to elucidate the effect of fluorination on the crystallization behaviors of parent polyurethanes without the interaction between hard segment and soft segment. This study prepared the aliphatic fluorinated polyurethane based on hexamethylene diisocyanate (HDI) and 2,2,3,3-tetrafluoror-1,4-butanediol. The aliphatic nonfluorinated polyurethane based on HDI and 1,4-butandiol (BD) was also synthesized for comparison. The effects of fluorocarbon chains on the solubility behavior, microstructure, thermal transition property, and crystal morphology were studied using Fourier transfer infrared spectrophotometry, wide-angle X-ray diffraction, differential scanning calorimetry, and polarized optical microscopy. An investigation of the isothermal crystallization kinetics of the polyurethanes was carried out using a differential scanning calorimeter.

EXPERIMENTAL

Materials

1,4-Butanediol (BD; Tedia, Fairfield, OH) and dimethylacetamide (DMAc; Tedia) were vacuum distilled over calcium hydride and then dried over 4 Å molecular sieves prior to use. 2,2,3,3-Tetrafluoro-1,4-butanediol (TF; Lancaster, Lancashire, UK) was dehydrated under vacuum at 50°C for 24 h before use. Hexamethylene diisocyanate (HDI; Aldrich, Milwaukee, WI) and stannous octoate (T-9; Sigma, St. Louis, MO) were used as received.

Synthesis

HDI was dissolved in DMAc in a four-necked flask under a nitrogen atmosphere and an equimolar amount of TF/DMAc or BD/DMAc solution was added dropwise at 70°C. After TF/DMAc or BD/DMAc solution was added, the temperature was raised to 90°C. Because of the lower reactivity of TF compared with BD, the content of stannous octoate as catalyst was 1.5 and 1 wt %, respectively. Reaction completion was monitored by the absence of free NCO group absorption at 2270 cm^{-1} by Fourier transfer infrared spectrophotometry (FTIR). Polyurethanes obtained were precipitated in deionized water, washed thoroughly with methanol, and dried in a vacuum oven at 60°C for 1 week. Fluorine-containing polyurethane obtained by reacting HDI with TF was designated as HDITF, whereas the corresponding fluorine-free polyurethane obtained by reacting HDI with BD was designated as HDIBD.

Characterization

Elemental analysis was performed on a Heraeus CHN-Rapid Elemental Analyzer to determine the amount of carbon, hydrogen, and nitrogen atoms.

Inherent viscosities were measured in DMAc solution at 50°C using an Ubbelohde type viscometer.

Infrared survey spectra were recorded with FTIR (Bio-Rad FTS-40A) operated with a dry air purge. Sixty-four scans at a resolution of 2 cm^{-1} were averaged. The samples for infrared analysis were prepared by solution casting of 1% (W/V) polymer in DMAc directly onto KBr plates and dried at 70°C. Following evaporation of most of the solvent, the samples were placed in a vacuum oven at 60°C for 24 h to remove the residual solvent.

Wide-angle X-ray diffraction (WAXD) measurements were performed on a Rigaku D/max 3.VX-Ray diffractometer with monochromatic Cu K_α radiation ($\lambda = 1.542$ Å). Data were collected from 3° to 35° (2θ).

Differential scanning calorimetry measurement

A Dupont DSC 2910 differential scanning calorimeter (DSC) and refrigerated cooling system (RCS) cooling system were used to determine the thermal transition. The samples were heated to 200°C, maintained at 200°C for 5 min, cooled to 0°C, maintained

TABLE I
Elemental Analysis of the Polyurethanes

	C %		H %		N %	
Sample	Calcd.	Found	Calcd.	Found	Calcd.	Found
HDITF	43.64	43.55	5.45	5.50	8.48	8.56
HDIBD	55.81	55.72	8.53	8.48	10.85	10.94

at 0°C for 5 min, and reheated once again. The scanning rate was 10°C/min. The cooling and second heating scans were recorded.

A Perkin–Elmer DSC 7 differential scanning calorimeter was used for isothermal crystallization measurements. Each sample was heated to 210°C for 5 min to erase the thermal history then rapidly cooled at 200°C/min to the desired crystallization temperature. The isothermal crystallization exotherm was recorded as a function of time. Subsequently each sample was heated at a rate of 10°C/min to 210°C to obtain the melting curves.

Polarized optical microscopy

The crystal morphology of polyurethanes was observed via an Olympus BH-2 polarizing optical microscope equipped with a Linkam Scientific Instruments CI 93 temperature controller and a THMS 600 hot stage. HDIBD and HDITF were first melted for 5 min at 210 and 200°C, respectively, and then rapidly cooled at 130°C/min to the desired crystallization temperature to observe the crystal morphology.

RESULTS AND DISCUSSION

The chemical repeating units of HDITF and HDIBD can be depicted as follows:

$$[CONH(CH_2)_6NHCOOCH_2(CF_2)_2CH_2O]_n \quad \text{HDITF}$$

$$[CONH(CH_2)_6NHCOO(CH_2)_4O]_n \quad \text{HDIBD}$$

Table I shows the elemental analysis data of polyurethanes studied. Obviously, the compositions of polyurethanes obtained are in good agreement with those predicted.

The inherent viscosities of HDITF and HDIBD in DMAc at 50°C are 0.38 and 0.52 dL/g, respectively. The result indicates that there is a decrease in the viscosity after introducing $(CF_2)_2$ moieties in polyurethane.

Solubility was determined at concentrations of 1 g/100 mL. HDITF is readily soluble in DMAc, DMF, and DMSO at room temperature (30°C). On the contrary, HDIBD is only soluble in DMAc, DMF, and DMSO above a temperature of about 45, 70, and 45°C, respectively. The solubility behavior clearly indicates that the introduction of $(CF_2)_2$ moieties apparently improved the solubility of the polyurethane, due to the disruption of polymer chain packing, as is often the case for fluorine-containing polyamides.[20–22]

Infrared spectroscopy analysis

The FTIR absorption spectra of the polyurethanes recorded at room temperature are shown in Figure 1. The absorption band observed at 1185 cm^{-1} (C—F stretching) indicates the presence of fluorocarbon chains in HDITF. In addition, another absorption band for the C—F stretching overlaps with the one for the C—O—C stretching at 1137 cm^{-1}. The hydrogen-bonded carbonyl absorption bands of HDITF and HDIBD occur at 1704 and 1685 cm^{-1}, respectively. The hydrogen-bonded N—H absorption bands of HDITF and HDIBD are located at 3340 and 3321 cm^{-1}, respectively. The free N—H band of HDITF appears as a shoulder at 3453 cm^{-1}, however, that of HDIBD is hardly observed. The hydrogen-bonded carbonyl and N—H band positions of HDITF are shifted to higher frequencies compared with those of HDIBD. This shift might be ascribed to a decrease in the bond electron density of the carbonyl and N—H groups[23] or weakening of hydrogen bonding by substitution of fluorine atoms in CH_2

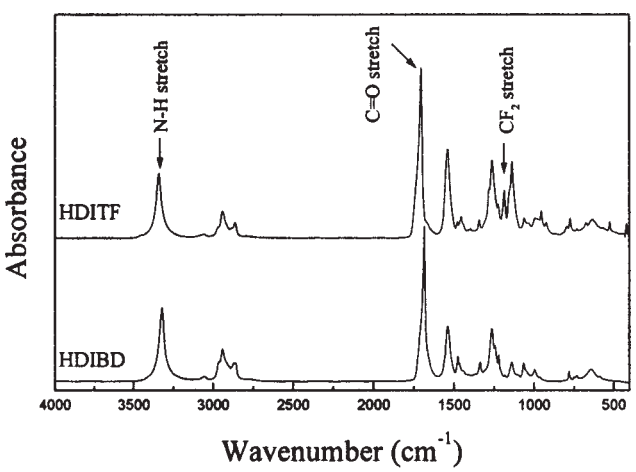

Figure 1 FTIR spectra of the polyurethanes.

TABLE II
Results of the Deconvolution of the Carbonyl Groups

	Hydrogen bonded											
	Ordered			Disordered			Free					
Sample	ν (cm^{-1})	$W_{1/2}$ (cm^{-1})	A_o	ν (cm^{-1})	$W_{1/2}$ (cm^{-1})	A_d	ν (cm^{-1})	$W_{1/2}$ (cm^{-1})	A_f	A_o/A_T (%)	A_d/A_T (%)	A_f/A_T (%)
HDITF	1704	7.0	5.0	1718	15.7	9.2	1745	12.1	2.3	30.3	55.8	13.9
HDIBD	1685	7.0	6.5	1701	13.6	7.4	1725	11.3	1.8	41.4	47.1	11.5

ν, frequency; $W_{1/2,}$ width at half-height; A_o, area (arbitrary units) of carbonyl sub-band attributed to ordered domains; A_d, area of carbonyl sub-band attributed to disordered domains; A_f, area of carbonyl sub-band attributed to free carbonyl groups; $A_{T,}$ total area of carbonyl band ($A_T = A_o + A_d + A_f$).

groups.[24] Deconvolution of the carbonyl stretching region based on the Gaussian function was performed.[25] Three bands could be resolved. The results of the deconvolution of the carbonyl stretching region are listed in Table II. HDITF shows the bands at 1704, 1718, and 1745 cm^{-1}, which can be attributed to the ordered, disordered hydrogen-bonded, and free carbonyls, respectively. However, HDIBD exhibits the bands at 1685, 1701, and 1725 cm^{-1} instead. The quantitative analysis of each mode of carbonyls was obtained if they were assumed to have approximately the same extinction coefficient. As shown in Table II, HDITF contains larger fractions of disordered hydrogen-bonded and free carbonyls but a smaller fraction of ordered hydrogen-bonded carbonyls than HDIBD. Further, the free N—H band is observed as a shoulder on the *N*-H stretching region of HDITF, however, that is hardly observed for HDIBD. These results imply that the $(CF_2)_2$ moieties do not in favor the ordered domains and hydrogen bonding between N—H and carbonyls compared with $(CH_2)_2$ moieties, due to the disruption of polymer chain packing, as mentioned in the above solubility behavior. Consequently, the arrangement of molecular chains for HDITF is less regular than HDIBD.

Wide-angle X-ray diffraction

The WAXD patterns of the polyurethanes recorded at room temperature are shown in Figure 2. HDITF exhibits the broad peaks around $2\theta \approx 22.5°$, 21.2°, 20.7°, 19.0°, and 6.5°, which correspond to 4.0, 4.2, 4.3, 4.7, and 13.6 Å in *d* spacing as calculated by the Bragg equation. The diffraction peak at $2\theta \approx 6.5°$ corresponds to fiber axis periodicity.[24] Wang[26] synthesized fluorinated aliphatic polyurethanes using HDI, poly(tetramethyl oxide), and TF. A diffraction peak at $2\theta \approx 6.3°$ came from the reflection of structure repeat (*c*-axis). HDIBD presents a sharp peak around $2\theta \approx 24.4°$ and broad peaks around $2\theta \approx 22.4°$, 21.9°, 20.7°, and 13.8°, which correspond to 3.6, 4.0, 4.1, 4.3, and 6.4 Å in *d* spacing. The WAXD patterns reflect that the positions of the peaks are changed, suggesting the crystal structure change associated with the $(CF_2)_2$ moieties in place of $(CH_2)_2$ moieties. Moreover, the crystallinity reflection of HDIBD is more prominent than HDITF, suggesting a higher degree of crystallinity for HDIBD. Steinhauser and Mülhaupt [20] prepared fluorine-containing copolyamides using oligo(tetrafluoroethylene) segments. As content and segment length of the oligo(tetrafluoroethylene) segments increased, the crystallinity was reduced markedly. Kiyotsukuri et al.[22] also found that the incorporation of fluorine substituents into copolyamides reduced the crystallinity.

Thermal transition behaviors

The cooling and second heating curves of the polyurethanes are presented in Figure 3. The melting temperature (T_m), crystallization temperature (T_c), heat of fusion (ΔH_f), and entropy of fusion (ΔS_f) are listed in Table III. For exothermic and endothermic processes, the peak temperatures were taken as the transition temperatures. HDITF has lower transition temperatures than HDIBD. This is in good agreement with the previous studies by many investigators[20–22] in which the fluorine-containing polyamides had lower melting temperatures than the corresponding fluorine-free polyamides. This might be attributed to the disruption of polymer chain

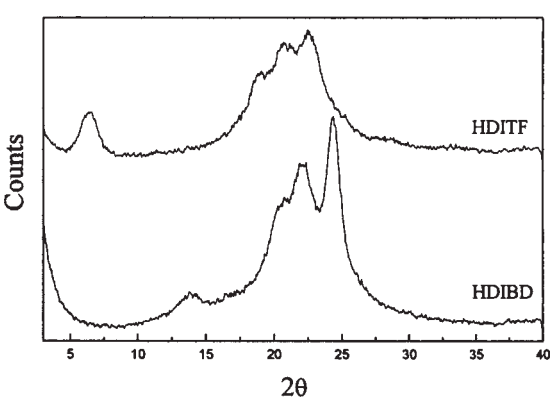

Figure 2 WAXD spectra of the polyurethanes.

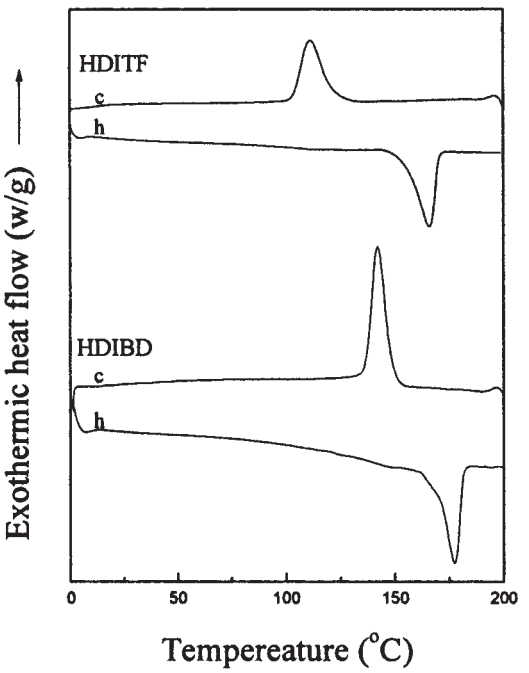

Figure 3 Cooling (c) and heating (h) DSC traces of the polyurethanes.

packing by the introduction of the fluorocarbon chains, as observed in FTIR analysis. The values of ΔH_f for HDITF and HDIBD are 50 and 71 J/g, respectively, whereas the values of ΔS_f calculated by the equation $\Delta S_f = \Delta H_f/T_m$ are 0.30 and 0.40 J/g°C for HDITF and HDIBD, respectively. The smaller ΔH_f of HDITF is probably due to the weak intermolecular cohesion energy of fluorine constituent, while the smaller ΔS_f of HDITF might be attributed to the rigid-rod-like nature of the fluorocarbon segments.

Crystal morphology

Figure 4 presents the crystal morphology of polyurethanes, which was conducted by polarizing microscopy. Crystallization of HDITF and HDIBD was carried out at 130 and 156°C, respectively. The polyurethanes show to crystallize into a variety of spherulitic forms. A bright, birefringent and spherulitic texture is observed for HDIBD. Moreover, a classic maltese cross pattern is seen on the spherulitic texture. On the other hand, the broad banding rings on a maltese cross pattern are observed for HDITF. These rings are suggested to arise from a regular twist of lamellae in the radial direction of the spherulite, which might be caused by the bulky $(CF_2)_2$ moieties.

TABLE III
Thermal Transition Temperatures of the Polyurethanes

Sample	T_m (°C)	ΔH_f (J/g)	ΔS_f (J/g °C)	T_c (°C)
HDITF	166	50	0.30	112
HDIBD	177	71	0.40	142

Analysis of the isothermal crystallization kinetics

The isothermal crystallization kinetics of polymers has been interpreted in terms of the Avrami equation[27,28]:

$$1 - X_t = \exp(-Kt^n) \quad (1)$$

where X_t is the relative crystallinity at time t, K is the overall crystallization rate constant involving contributions from crystal growth and nucleation, and n is the Avrami exponent, which contains contributions related to the crystal growth geometry, the mechanism of nucleation, and the growth control factor. The half-time of crystallization ($t_{1/2}$) defined as the time to a relative crystallinity of 50%, is related to the rate constant and can be determined from the Avrami expression as follows:

$$t_{1/2} = (\ln 2/K)^{1/n} \quad (2)$$

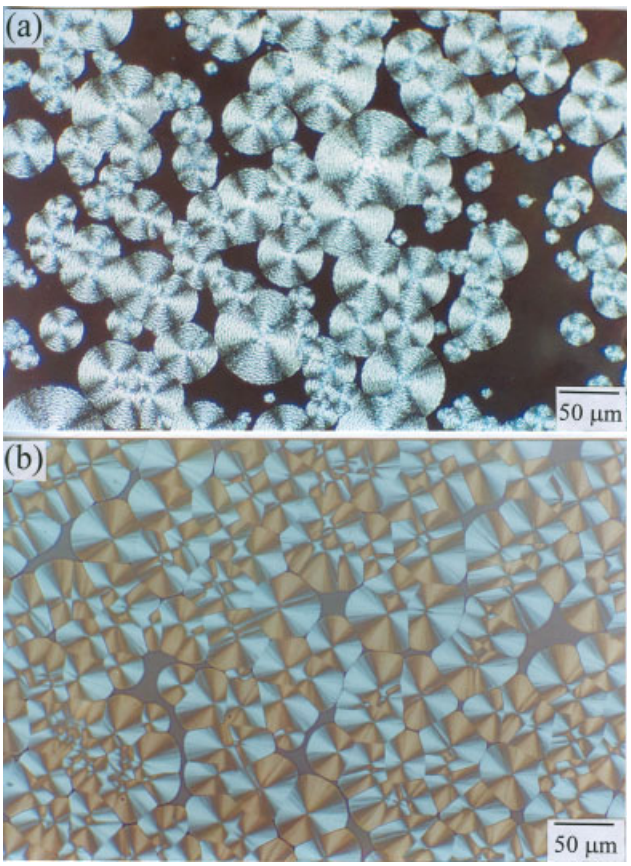

Figure 4 Optical microscope photographs of the polyurethanes after crystallization at different temperature: (a) HDITF at 130°C; (b) HDIBD at 156°C. [Color figure can be viewed in the online issue, which is available at www.interscience.wiley.com.]

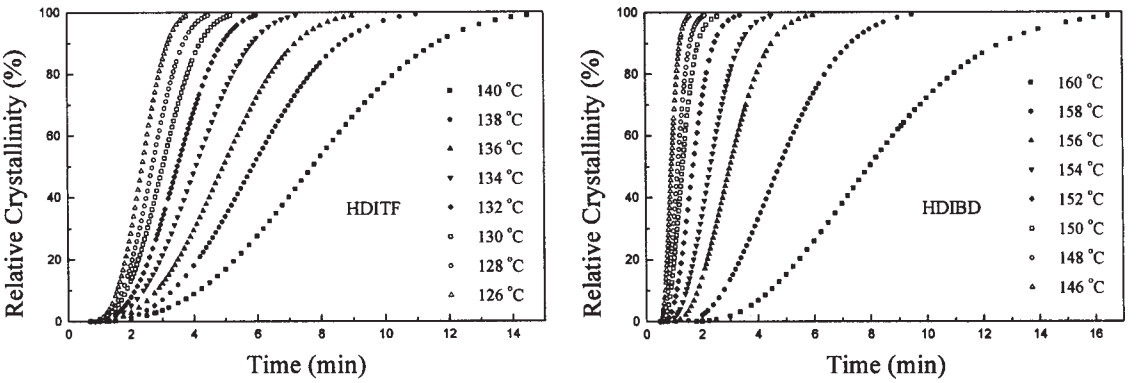

Figure 5 Relative crystallinity of the polyurethanes at different crystallization temperatures as a function of time.

Differentiating eq. (1) twice, and when $d^2X_t/dt^2 = 0$, the time to reach the maximum heat flow (t_{max}) can be obtained:

$$t_{max} = [(n-1)/nK]^{1/n} \quad (3)$$

The isothermal crystallization of HDITF and HDIBD was carried out in the temperature range of 140 to 126°C and 160 to 146°C, respectively. By following the Avrami treatment, the relative crystallinity versus time for HDITF and HDIBD at different crystallization temperatures is calculated in Figure 5. The typical Avrami plots for HDITF and HDIBD obtained at different crystallization temperatures are illustrated in Figure 6. There are good linearities of $\log[-\ln(1 - X_t)]$ versus $\log t$ in a relative crystallinity range of 5 to 80%. The Avrami exponent (n) and the overall crystallization rate constant (K) are obtained from the values of the slope and intercept of these straight lines. The isothermal crystallization kinetics parameters are determined and summarized in Table IV. The values of K increase with decreasing crystallization temperature (T_c). From Table IV, it can be seen that the values of $t_{1/2}$ and t_{max} obtained from experimental data are consistent with those calculated from eqs. (2) and (3), indicating the validity of the Avrami equation in this study. The peak time of the crystallization exotherm t_{max} which represents reciprocally the overall rate of crystallization increases with increasing temperature of isothermal crystallization, i.e., the rate of crystallization decreases with increasing crystallization temperature. As expected the $t_{1/2}$ also increases with increasing crystallization temperature. In this study, the isothermal crystallization for HDITF and HDIBD was carried out in different temperature range. However, by comparing the t_{max}, $t_{1/2}$, and K for HDITF at 140°C with those for HDIBD at 146°C, one can see that the overall rate of crystallization of HDITF will be lower than that for HDIBD if they crystallize at the same temperature. The values of n for HDITF and HDIBD are in the range of 2.33 to 2.78 and 2.16 to 2.59, respectively, depending on the crystallization temperature. They are close to 2.5, which indicates the growth of crystal might be spherulite growth corresponding to homogeneous (thermal) nucleation and diffusion-controlled growth.[29] This result is similar to that of MacKnight et al.[19] They showed that the Avrami exponent of poly(4,4′-bis(6-hydroxyhexoxy)biphenyl-2,4-toluenediisocyanate) for crystallization from the isotropic melt is 2.6.

The melting endotherms of HDITF and HDIBD after isothermal crystallization at different temperatures are shown in Figure 7. The sample was heated

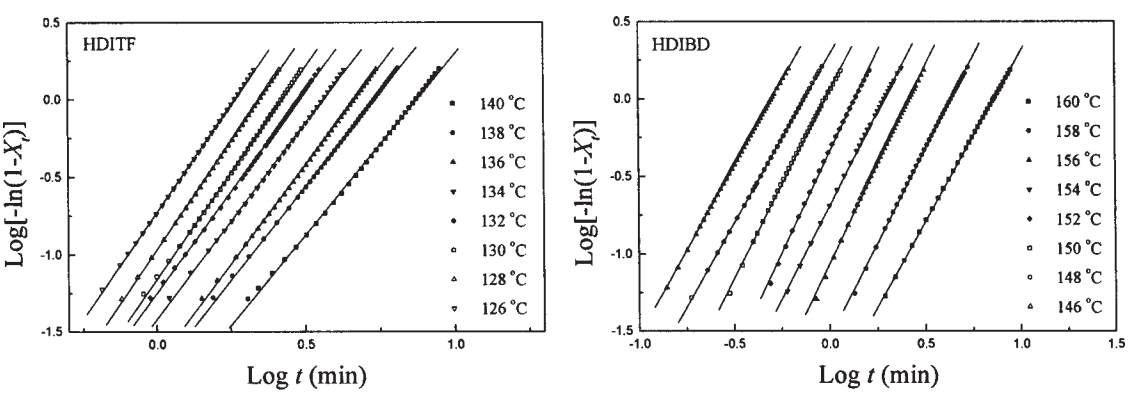

Figure 6 Avrami plots of the polyurethanes at different crystallization temperatures.

TABLE IV
Results of Isothermal Crystallization Kinetic Parameters

T_c (°C)	n	K (min^{-1})	$t_{1/2}$[a] (min)	$t_{1/2}$[b] (min)	t_{max}[a] (min)	t_{max}[c] (min)
HDITF						
140	2.33	9.05×10^{-3}	6.45	6.44	6.38	5.92
138	2.42	1.70×10^{-2}	4.68	4.63	4.43	4.32
136	2.55	1.99×10^{-2}	4.00	4.02	3.87	3.82
134	2.52	3.81×10^{-2}	3.23	3.16	3.19	2.99
132	2.59	5.61×10^{-2}	2.79	2.64	2.75	2.52
130	2.73	6.87×10^{-2}	2.34	2.33	2.32	2.26
128	2.78	1.06×10^{-1}	1.97	1.96	1.96	1.91
126	2.74	1.85×10^{-1}	1.62	1.62	1.61	1.57
HDIBD						
160	2.20	1.28×10^{-2}	6.17	6.14	5.61	5.50
158	2.41	2.90×10^{-2}	3.73	3.73	3.36	3.48
156	2.55	8.55×10^{-2}	2.27	2.27	2.10	2.16
154	2.39	2.01×10^{-1}	1.67	1.68	1.51	1.56
152	2.59	4.43×10^{-1}	1.18	1.19	1.07	1.13
150	2.41	1.10	0.82	0.83	0.74	0.77
148	2.16	1.87	0.63	0.63	0.58	0.56
146	2.17	4.45	0.43	0.43	0.37	0.38

[a] Obtained from experimental data.
[b] Calculated from Eq. (2).
[c] Calculated from Eq. (3).

at a rate of 10°C/min from the crystallization temperature to 210°C. From Figure 7, a multiple melting point phenomenon was observed for HDITF and HDIBD. HDITF displays a distinct melting peak, shoulder peak, and smaller peak, which are labeled as Peak I, Peak II, and Peak III, respectively. The position of the melting Peak I, which appears at higher temperature, seems to be independent of the crystallization temperature. By contrast, the melting temperatures of Peaks II and III, which appear at lower temperatures, are strongly dependent on the crystallization temperature used, increasing with increasing crystallization temperature. Moreover, the intensity ratio of Peak II/Peak I increases with increasing crystallization temperature. HDIBD shows a melting peak and shoulder, which are labeled as Peak I and Peak II, respectively, in the crystallization temperature range of 160 to 154°C. Note that in addition to these two peaks, the melting endotherm show a third melting peak or shoulder, which is labeled as Peak III, in the crystallization temperature range of 152 to 146°C. The intensity ratio of Peak III/Peak I increases with decreasing crystallization temperature. The melting temperatures of the Peak I and Peak II increase with increasing crystallization temperature. However, the position of the melting Peak III is not influenced by crystallization temperature. These results are in consistent with the results observed in the isothermal crystallization studies of nylons.[30–34] The multiple melting behavior could be attributed to a melting–recrystallization–remelting process during a heating scan.[30,32] An endothermic peak at a temperature close to its crystallization temperature is due to the annealing effects in the crystallization process or the microcrystallite formation in the boundary layer between the larger crystallities.[30,32–34] The Peak II for HDITF and Peak I for HDIBD result from the melting of lamellae with different thickness developing under different crystallization conditions, while the Peak I for HDITF and Peak III for HDIBD originate from the melting of the recrystallized crystals.[30,32] With an increase of the crystallization temperature, the crystals become thickened and more perfect, so the Peak II for HDITF and Peak I for HDIBD are shifted to higher temperature. However, the final melting of recrystallized material takes place at the same temperature. The Peak III for HDIBD disappears in the crystallization temperature above 154°C, indicating that no further recrystallization can occur during heating.[30]

The isothermal crystallization temperature was found to affect the melting behavior of HDITF and HDIBD in the above DSC analysis. Furthermore, the effect of the isothermal crystallization temperature on the crystalline structure of HDITF and HDIBD was investigated by WAXD. The samples were heated to 210°C for 5 min, rapidly cooled at 200°C/min to the same crystallization temperature as the above isothermal crystallization analysis, annealed for 1 h, and then rapidly cooled at 200°C/min to 30°C. Figure 8 exhibits that the WAXD patterns of HDITF and HDIBD are independent of isothermal crystallization temperatures. This result indicates that the crystalline structures are not changed in the

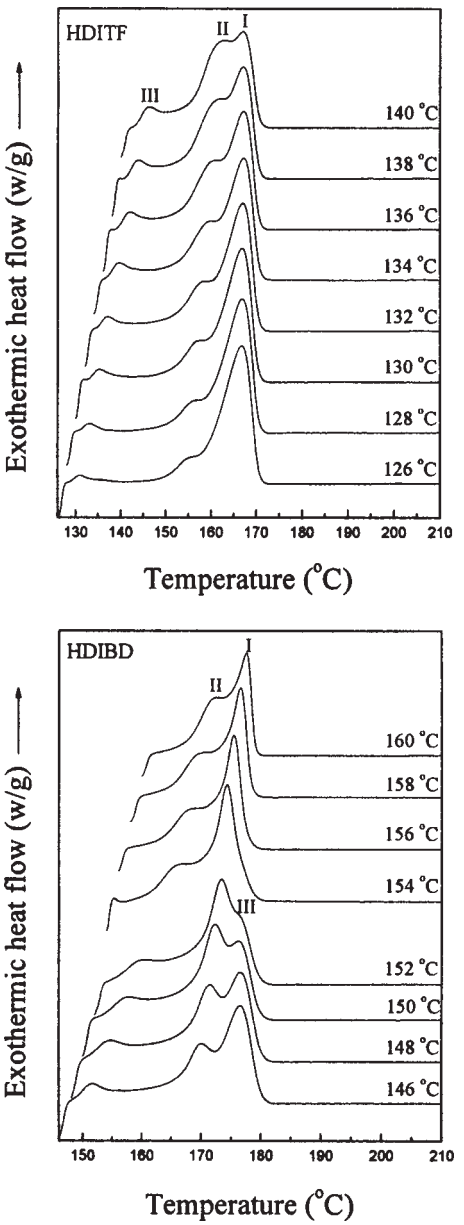

Figure 7 DSC thermographs of the polyurethanes after isothermal crystallization at different temperatures.

isothermal crystallization temperature range of this study. Therefore, the possibility that the multiple endotherms resulted from different crystalline forms can be ruled out.[30,32] The multiple endotherms are due to the melting of the recrystallizated materials or the lamellae produced under different crystallization processes. The melting temperature increased with increasing crystallization temperature, indicating that more perfect crystals have formed at higher crystallization temperature.[31]

Analysis of crystallization activation energy

The crystallization process for HDITF and HDIBD is assumed to be thermally activated, then the overall crystallization rate K can be approximately described by the Arrhenius equation as the following form[35–37]:

$$K^{1/n} = k_0 \exp(-\Delta E/RT_c) \tag{4}$$

$$(1/n)\ln K = \ln k_0 - \Delta E/RT_c \tag{5}$$

where k_0 is a temperature-independent pre-exponential factor, ΔE is the crystallization activation energy, and R is the universal gas constant, the rest of the parameters have meanings as above-mentioned. According to the values of n, K, and T_c in Table IV, the slopes of plots of $(1/n)\ln K$ versus $1000/T_c$ will give $\Delta E/R$ (Fig. 9). The value of ΔE is found to be -130.9 kJ/mol for HDITF, and -276.9 kJ/mol for HDIBD. The value of ΔE is negative because it has

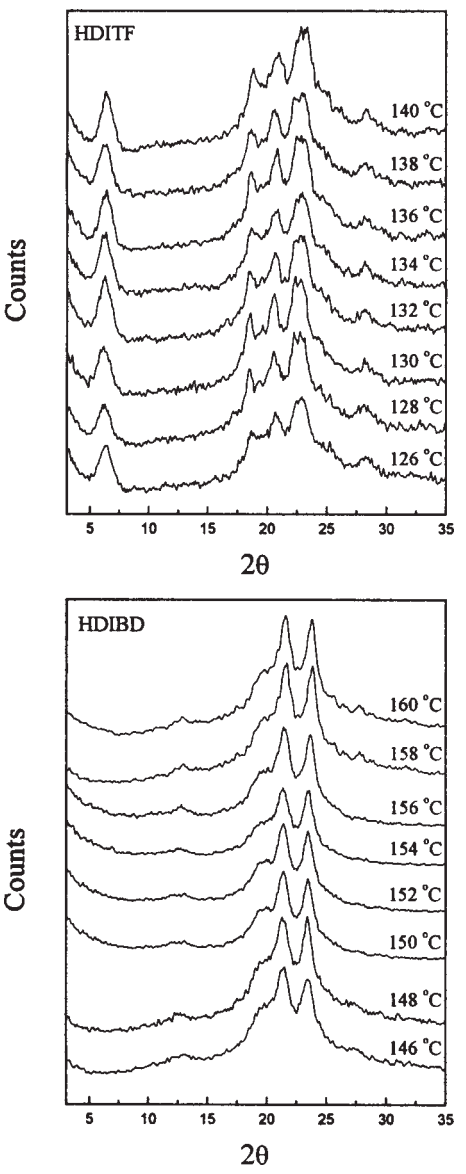

Figure 8 WAXD spectra of the polyurethanes after isothermal crystallization at different temperatures for 1 h.

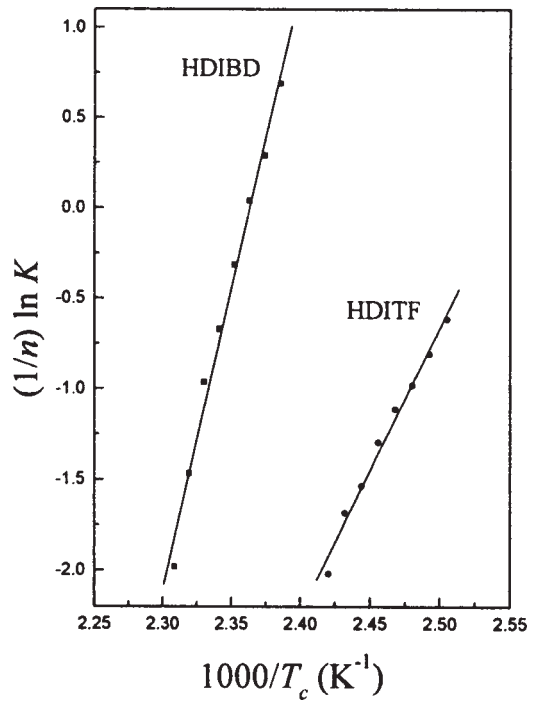

Figure 9 Arrhenius plots of $(1/n)\ln K$ versus $1000/T_c$.

to release energy while transforming the molten fluid into the crystalline state. It is noted that ΔE for HDITF is lower in magnitude than that for HDIBD. This indicates that HDITF releases less energy than HDIBD when it transforms from the molten fluid into the ordered crystalline state, which is consistent with the FTIR results that the arrangement of molecular chains for HDITF is less regular than HDIBD.

CONCLUSIONS

In this study, the fluorinated polyurethane, HDITF, exhibits a lower viscosity, higher solubility in organic solvents including DMAc, DMF, and DMSO, smaller fraction of ordered hydrogen-bonded carbonyls, and lower transition temperatures than the corresponding fluorine-free polyurethane, HDIBD, due to the disruption of polymer chain packing by the fluorocarbon chains. The wide-angle X-ray diffraction patterns reflect change of crystal structure with the $(CF_2)_2$ moieties in place of $(CH_2)_2$ moieties. Polarized optical microscopy also reveals that the polyurethanes crystallize into a variety of spherulitic forms.

The isothermal kinetics of the polyurethanes was interpreted in terms of the Avrami equation. The Avrami exponent (n) for the polyurethanes is about 2.5, which indicates the growth of crystal might be spherulite growth corresponding to homogeneous (thermal) nucleation and diffusion control. HDITF has a lower crystallization activation energy than HDIBD because the molecular chains of HDITF are less regular than those of HDIBD.

References

1. Kawakami, H.; Mikawa, M.; Takagi, J.; Nagaoka, S. J Biomater Sci Polym En 1996, 7, 1029.
2. Furukawa, M. J Appl Polym Sci Appl Polym Symp 1994, 53, 61.
3. Tonelli, C.; Trombetta, T.; Scicchitano, M.; Castiglioni, G. J Appl Polym Sci 1995, 57, 1031.
4. Ho, T.; Wynne, K. J. Macromolecules 1992, 25, 3521.
5. Honeychuck, R. V.; Ho, T.; Wynne K. J. Nissan, R. A. Chem Mater 1993, 5, 1299.
6. Kashiwagi, T.; Ito, Y.; Imanishi, Y. J Biomater Sci Polymer En 1993, 5, 157.
7. Tonelli, C.; Trombetta, T.; Scicchitano, M.; Simeone, G.; Ajroldi, G. J Appl Polym Sci 1996, 59, 311.
8. Tonelli, C.; Ajroldi, G. J Appl Polym Sci 2003, 87, 2279.
9. Tang, Y. W.; Santerre, J. P.; Labow, R. S.; Taylor, D. G. J Biomed Mater Res 1997, 35, 371.
10. Jahangir, A. R.; McClung, W. G.; Cornelius, R. M.; McCloskey, C. B.; Brash, J. L.; Santerre, J. P. J Biomed Mater Res 2002, 60, 135.
11. Massa, T. M.; McClung, W. G.; Yang, M. L.; Ho, J. Y. C.; Brash, J. L.; Santerre, J. P. J Biomed Mater Res 2007, 81A, 178.
12. Lin, Y. H.; Chou, N. K.; Chang, C. H.; Wang, S. S.; Chu, S. H.; Hsieh, K. H. J Polym Sci Part A: Polym Chem 2007, 45, 3231.
13. Wang, L. F.; Wei, Y. H. Colloid Surface B 2005, 41, 249.
14. Wang, L. F. Eur Polym J 2005, 41, 293.
15. Chen, K. Y.; Kuo, J. F. Macromol Chem Phys 2000, 201, 2676.
16. Bogdanov, B.; Toncheva, V.; Schacht, E.; Finelli, L.; Sarti, B.; Scandola, M. Polymer 1999, 40, 3171.
17. Zhu, Y.; Hu, J. L.; Yeung, K. W.; Liu, Y. Q.; Liem, H. M. J Appl Polym Sci 2006, 100, 4603.
18. Zhu, Y.; Hu, J. L.; Choi, K. F.; Yeung, K. W.; Meng, Q.; Chen, S. J Appl Polym Sci 2008, 107, 599.
19. Smyth, G.; Valles, E. M.; Pollack, S. K.; Grebowicz, J.; Stenhouse, P. J.; Hsu, S. L.; MacKnight, W. J Macromolecules 1990, 23, 3389.
20. Steinhauser, N.; Mülhaupt, R. Macromol Chem Phys 1994, 195, 3199.
21. Yoneyama, M.; Yamazaki, K.; Kakimoto, M.; Imai, Y. Macromol Chem Phys 1999, 200, 2208.
22. Kiyotsukuri, T.; Tsutsumi, N.; Sandan, T. J Polym Sci Part A: Polym Chem 1990, 28, 315.
23. Yoon, S. C.; Ratner, B. D. Macromolecules 1988, 21, 2392.
24. Jayasuriya, A. C.; Tasaka, S.; Shouko, T.; Inagaki, N. Polym J 1995, 27, 122.
25. Teo, L. S.; Chen, C. Y.; Kuo, J. F. Macromolecules 1997, 30, 1793.
26. Wang, L. F. Polymer 2007, 48, 7414.
27. Avrami, M. J Chem Phys 1939, 7, 1103.
28. Avrami, M. J Chem Phys 1940, 8, 212.
29. Wunderlich, B. Macromolecular Physics; Academic Press: New York, 1976; Vol. 2.
30. Zhang, X.; Xie, T.; Yang, G. Polymer 2006, 47, 2116.
31. Zheng, L. J.; Qi, J. G.; Zhang, Q. H.; Zhon, W. F.; Liu, D. J Appl Polym Sci 2008, 108, 650.
32. Ren, M.; Mo, Z.; Chen, Q.; Song, J.; Wang, S; Zhang, H.; Zhao, Q. Polymer 2004, 45, 3511.
33. Weng, W.; Chen, G.; Wu, D. Polymer 2003, 44, 8119.
34. Liu, M.; Zhao, Q.; Wang, Y.; Zhang, C.; Mo, Z.; Cao, S. Polymer 2003, 44, 2537.
35. Cebe, P.; Hong, S. D. Polymer 1986, 27, 1183.
36. Liu, S.; Yu, Y.; Cui, Y.; Zhang, H.; Mo, Z. J Appl Polym Sci 1998, 70, 2371.
37. Wang, C. S.; Lin, C. H. J Polym Sci Part B: Polym Phys 1999, 37, 2269.